Spin-orbit Torques and Magnetization Switching in Perpendicularly Magnetized Epitaxial Pd/Co_2FeAl/MgO Structures

M. S. Gabor,[1,*] T. Petrisor Jr,[1] M. Nasui,[1] M. A. Nsibi,[2] J. Nath,[2] and I. M. Miron[2,†]

[1] *Center for Superconductivity, Spintronics and Surface Science, Physics and Chemistry Department, Technical University of Cluj-Napoca, Str. Memorandumului, 400114 Cluj-Napoca, Romania*

[2] *Univ. Grenoble Alpes, CNRS, CEA, Grenoble INP, IRIG-Spintec, 38000 Grenoble, France*

(Received 14 August 2019; revised manuscript received 12 December 2019; accepted 21 April 2020; published 18 May 2020)

Epitaxial magnetic heterostructures of MgO(001)//Pd/Co_2FeAl/MgO are grown by magnetron sputtering and the current-induced spin-orbit torques are quantified using harmonic Hall measurements. We demonstrate efficient current-induced spin-orbit-torque switching in perpendicularly magnetized samples. The advantage of such heterostructures for spin-orbit-torque magnetic random-access memory devices is that they allow a combination of critical ingredients: (i) the low resistivity required for reduced electric energy consumption during writing, (ii) the compatibility with a high tunnel magnetoresistive ratio required for efficient reading, and (iii) strong perpendicular magnetic anisotropy for increased thermal stability.

DOI: 10.1103/PhysRevApplied.13.054039

I. INTRODUCTION

Magnetization switching by current-induced spin-orbit torques (SOTs) in heavy-metal (HM) and ferromagnet (FM) heterostructures with perpendicular magnetic anisotropy (PMA) is of great research interest for the development of electrically controlled spintronic devices [1–5]. One application of the SOTs is three-terminal SOT magnetic random-access memory (MRAM). In this type of device, the information is written by switching the magnetization of the FM layer using current-induced SOTs in a bottom HM and FM electrode, while the information is read using a top magnetic tunnel junction (MTJ) structure [1,3]. The HMs used in this type of device fall into two categories: high resistivity, such as β-Ta [2,3,5–10] or β-W [10–16], and low resistivity, such as Pt [1,4,8,10,17–19] or Pd [20,21]. While in-plane magnetized three-terminal devices have been fabricated using Pt-based structures [22,23], perpendicular magnetized three-terminal devices demonstrated so far are based on either Ta/(Co, Fe)B/MgO [3,24] or W/(Co, Fe)B/MgO [25]. The reason is that they usually grow without a preferred orientation, or even in an amorphous state. This allows the (001) crystallization at the (Co, Fe)B/MgO interface during subsequent annealing stages, which is essential to achieve a high magnetoresistive ratio [26,27] and a strong PMA [28]. However, the use of low-resistivity HMs (Pt or Pd) is more desirable, because it reduces the Ohmic losses. The difficulty is that, when grown directly on Si/SiO_2 substrate or on a Ta buffer layer, the (111) fcc crystal face is energetically favorable and thus the (111) texturing is promoted. This constitutes an important impediment, because the (111) orientation of the HM it is not compatible with the required (001) texturing for the upper FM layer.

Our approach is to use HM and FM materials, which are (001) structural compatible, and grow (001) epitaxial HM and FM structures on a (001) MgO template. For the HM layer we use Pd, which has already been shown to produce relatively large SOTs [21], and which, unlike Pt, can exhibit (001) growth on MgO. As the ferromagnet, we use Co_2FeAl (CFA), a Co-based full Heusler alloy [29], which has been shown to provide large magnetoresistive ratios in perpendicular magnetized MgO-based magnetic tunnel junctions [30,31]. Therefore, in this paper we demonstrate that fully (001) epitaxial Pd/Co_2FeAl/MgO heterostructures showing perpendicular magnetic anisotropy can be grown on (001)-oriented MgO substrates. We evidence large SOTs and efficient SOT-induced switching. Our results open an avenue for employing low resistivity HM in three-terminal SOT devices by using (001) structural compatible materials grown on textured templates.

A. Experiment

The studied samples consist of MgO (001)/Pd (t_{Pd})/CFA (t_{CFA})/MgO (1 nm)/Ta (2 nm) stacks. To obtain a complete analysis in terms of structural properties, SOT amplitudes and magnetization switching we vary the CFA thickness. Pd thickness is also varied in order to probe the thickness dependence of the SOTs. The samples are grown at room

*mihai.gabor@phys.utcluj.ro
†mihai.miron@cea.fr

temperature using a magnetron sputtering system having a base pressure lower than 2×10^{-8} Torr. The metallic layers are grown by dc sputtering under an Ar pressure of 1 mTorr, while the MgO layer is grown by rf sputtering under an Ar pressure of 10 mTorr. The 2-nm-thick Ta capping layer is deposited to protect the samples from oxidation due to atmospheric exposure. No annealing is performed after the sample deposition. The structure of the samples is characterized by XRD experiments using a four-circle diffractometer. For magnetotransport measurements the samples are processed by UV lithography and Ar ion milling into Hall bar devices with a channel size of $20\times10\ \mu m^2$.

II. RESULTS AND DISCUSSIONS

The XRD measurements are performed on relatively thick Pd (8 nm)/CFA (10 nm)/MgO (1 nm) samples; they allow us to verify that the growth is epitaxial. Since the epitaxial growth is initiated at the MgO/Pd interface, our observation that the thick samples are epitaxial implies that the thinner ones, which cannot be analyzed directly using conventional XRD, are also epitaxial. In order to quantify the spin-orbit torques, we decrease the CFA thickness down to 2 nm. This thickness is ideal for determining the SOTs using the harmonic Hall techniques for in-plane magnetized materials. A further decrease of thickness is required for our last experiment for which we need perpendicular magnetic anisotropy. Here, we probe the SOT magnetization switching using magneto-optical Kerr effect.

Figure 1(a) shows $2\theta/\omega$ x-ray diffraction patterns measured for the Pd (8 nm)/CFA (10 nm)/MgO (1 nm) sample. Besides the peak corresponding to the MgO substrate, the patterns show only the (002) and (004) CFA peaks and the (002) Pd one. This indicates an out-of-plane (00l) textured growth of the stack. Figure 1(b) shows φ-scan measurements for the CFA (022)-, Pd (022)-, and MgO (022)-type reflections, recorded at a tilt angle $\psi = 45°$. The fourfold symmetry of the (022) CFA and (022) Pd reflections proves that the films are also in-plane oriented. Moreover, the $\varphi = 45°$ angle separation between the CFA (022)- and the MgO (022)- and Pd (022)-type reflections indicates the epitaxial relation MgO(001)[100]/Pd(001)[100]/CFA(001)[110], which imply an in-plane 45° rotation of the CFA crystal lattice relative to the Pd and the MgO one, as sketched in the inset of Fig. 1(b).

In order to characterize the torques, we obtain in-plane magnetized samples by depositing stacks with a CFA-layer thickness of 2 nm. We also vary the thickness of the Pd layer from 1 to 10 nm. First, we evaluate the electrical resistivity of the samples. Figure 2(a) shows the electrical resistance of the structures as a function of the Pd-layer thickness, measured by the four-probe technique in patterned samples. To extract the resistivity of the Pd layer

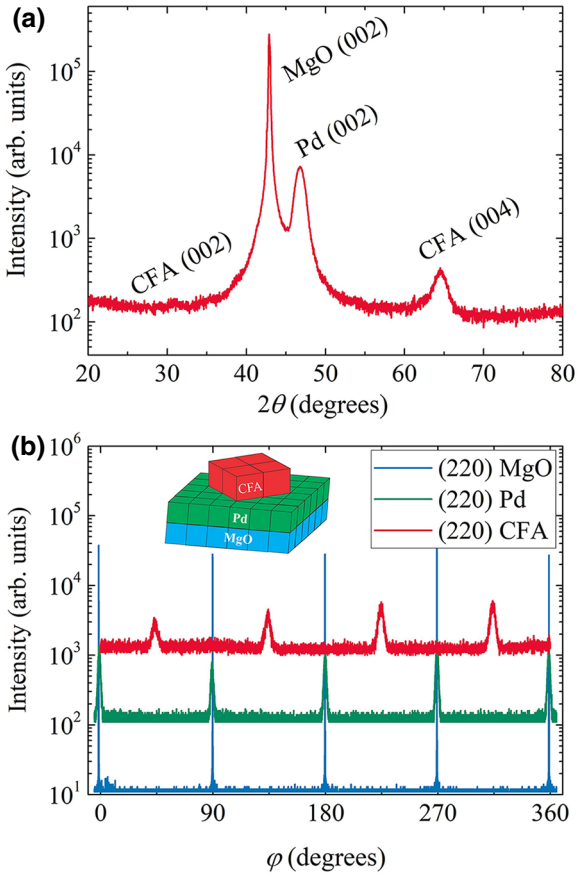

FIG. 1. (a) $2\theta/\omega$ x-ray diffraction pattern recorded for the Pd (8 nm)/CFA 10 nm/MgO (1 nm) sample. (b) φ-scan measurements for the CFA (022)-, Pd (022)-, and MgO (022)-type reflections. The inset shows a schematic of the CFA, Pd, and MgO crystals' lattice geometry.

we use a parallel resistor model in which we assume that the resistance of the CFA layer remains constant and that the Ta capping layer is fully oxidized and does not contribute to the conduction. The resistivity of the CFA layer is determined, by measuring the resistance of a patterned MgO/CFA(2 nm)/MgO(1 nm)/Ta(2 nm) sample, to be 170 $\mu\Omega$cm, in line with previous reports [32]. The inset of Fig. 2(a) depicts the Pd-layer resistivity variation on the inverse Pd thickness. A roughly linear dependence is observed, which allows us to calculate a relatively low bulk Pd resistivity ($t_{Pd} \to \infty$) of $\rho_{Pd}^{\infty} = 12\ \mu\Omega$cm, in agreement with previous reports [21]. To quantify the anomalous Hall resistance R_{AHE} and the effective anisotropy field H_k, we perform Hall measurements with the magnetic field H_z applied out of plane. R_{AHE} shows a strong decrease with the thickness of the Pd layer, predominantly due to the current shunting through Pd, while H_k remains rather constant at about 1.1 T [insets of Fig. 2(b)].

The SOTs are evaluated using the harmonic Hall method [8,33–35] established for in-plane magnetized films by

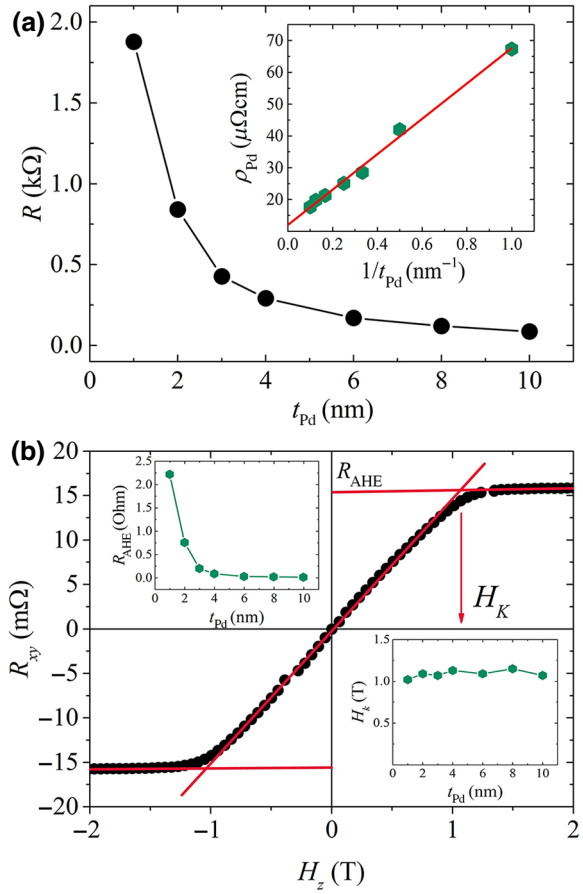

FIG. 2. (a) Electrical resistance of the Pd (t_{Pd})/CFA 2 nm/MgO (1 nm) structures as a function of the Pd-layer thickness. The inset depicts the Pd-layer resistivity dependence on the inverse Pd-layer thickness. (b) Typical anomalous Hall measurement performed with the magnetic field H_z applied out of plane. Insets show the dependences of the anomalous Hall resistance R_{AHE} and the effective anisotropy field H_k on the Pd-layer thickness.

Avci *et al*. [36], which has the advantage of providing a straightforward method of excluding the thermoelectric effects. The measurement geometry is shown in Fig. 3(a). The measurement technique consists in injecting an ac current ($I_\omega = I \sin \omega t$) into the patterned stripe (along $\hat{x}$) and measuring the first ($R_\omega = V_\omega/I$) and the second ($R_{2\omega} = V_{2\omega}/I$) harmonic Hall resistances (along $\hat{y}$), while rotating the magnetization in plane by applying an external in-plane rotating magnetic field (H_{ext}). Since the CFA films are in-plane magnetized, the R_ω provides information about the planar Hall effect as [36] $R_\omega = R_{\mathrm{PHE}} \sin 2\varphi$, where R_{PHE} is the planar Hall resistance and φ is the azimuthal angle of the magnetization from the current direction. Since the samples have a relatively weak in-plane uniaxial anisotropy, the φ azimuthal angle of the magnetization is practically identical to the φ_H azimuthal angle of the field [Fig. 3(a)]. The second harmonic Hall resistance $R_{2\omega}$ contains information about the SOT effective fields and it is given by [36]

$$R_{2\omega} = \left(\frac{1}{2} R_{\mathrm{AHE}} \frac{H_{\mathrm{DL}}}{H_{\mathrm{ext}} + H_k} + R_{\nabla T}\right) \cos\varphi + R_{\mathrm{PHE}}(2\cos^3\varphi - \cos\varphi) \frac{H_{\mathrm{FL}} + H_{\mathrm{Oe}}}{H_{\mathrm{ext}}},$$

where H_{DL} and H_{FL} are the dampinglike and fieldlike effective fields, $R_{\nabla T}$ is the second harmonic Hall resistance due to thermoelectric effects and H_{Oe} is the Oersted field produced by the charge current. By fitting the $R_{2\omega}$ experimental data to the above equation, two contributions can be extracted: one that shows a $\cos\varphi$ dependence, and another that shows a $2\cos^3\varphi - \cos\varphi$ dependence [Fig. 3(c)]. H_{DL} and $R_{\nabla T}$ are obtained from the slope and the intercept of the linear fit of the dependence of the $\cos\varphi$ contribution on the inverse of the sum of the external and anisotropy fields [Fig. 3(d)]. The sum $H_{\mathrm{FL}} + H_{\mathrm{Oe}}$ is determined from the slope of the linear fit of dependence of the $2\cos^3\varphi - \cos\varphi$ contribution on the inverse external field [Fig. 3(e)]. Finally, H_{Oe} is calculated as $H_{\mathrm{Oe}} = \mu_0 j_{\mathrm{Pd}} t_{\mathrm{Pd}}/2$, where j_{Pd} is the charge current density through the Pd layer and t_{Pd} is the thickness of the Pd layer, and it is subtracted from $H_{\mathrm{FL}} + H_{\mathrm{Oe}}$ sum to obtain H_{FL}.

Using the as-determined values for the H_{DL} and H_{FL} we calculate the SOT efficiency per charge current density through the Pd layer and per unit electric field (E), defined by [37]

$$\xi^{\mathrm{DL(FL)}}_{j_{\mathrm{Pd}}(E)} = \frac{2e}{\hbar} \mu_0 M_s t_{\mathrm{CFA}} \frac{H_{\mathrm{DL(FL)}}}{j_{\mathrm{Pd}}(E)},$$

where M_s is the saturation magnetization (10^6 A/m) and t_{CFA} is the thickness of the CFA layer (2 nm). We normalize the SOT effective fields to the electric field as well as to the charge current density through the Pd layer, in order to directly compare our results to literature data. The SOT efficiency values, which are shown in Fig. 4, are in agreement with the previously reported ones for the (111) textured Pd/Co/AlO_x system [21], indicating that CFA is a suitable ferromagnet for SOT switching. Irrespective of the normalization procedure, the SOT efficiencies show a monotonous increase with increasing the thickness of the Pd layer with no obvious saturation up to 10 nm. At the first glance, this dependence disagrees with the simple Rashba picture of interfacial torques. The spin-Hall-effect-generated torques scenario cannot be fully confirmed either, because we do not observe the saturation of the torques for large thickness. Larger thicknesses cannot be probed because the second harmonic SOT signal becomes too weak, due to the current shunting through the Pd layer.

Applications wise, the PMA samples are the ones to be used due to their higher thermal stability. Therefore, we probe SOT-induced magnetization switching in structures

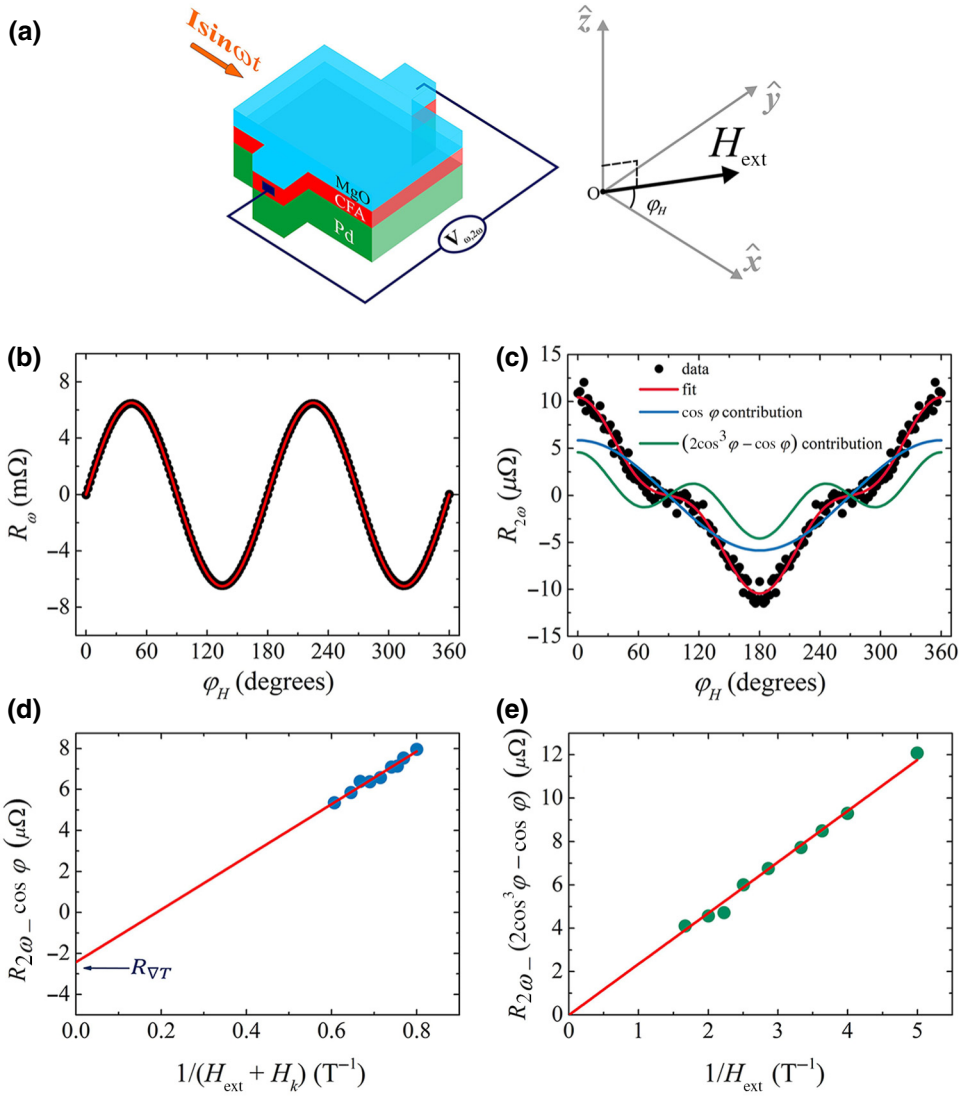

FIG. 3. (a) Schematic illustration of the Pd/CFA/MgO structure and harmonic Hall magnetotransport measurement geometry. (b) First- and (c) second-harmonic Hall resistances as a function of the azimuthal angle of the external in-plane magnetic field with the current direction, measured for a representative Pd (8 nm)/CFA (2 nm)/MgO (1 nm) sample. The points denote experimental data while the continuous lines are fits using the equations from the main text. Dependence of the second-harmonic Hall resistance (d) $\cos\varphi$ – contribution on $1/(H_{\text{ext}}+H_k)$ and (e) $2\cos^3\varphi - \cos\varphi$ – contribution on $1/H_{\text{ext}}$, used to extract the H_{DL} and the H_{FL}. The straight lines are linear fits to the data.

showing PMA. To obtain the PMA we fabricate samples having a CFA layer thickness of 0.9 nm. Figure 5 shows representative hysteresis loops measured with the magnetic field applied perpendicular or parallel to the sample surface. The out-of-plane loop shows a squared shape with full remanence, indicating that the CFA films are out-of-plane magnetized. Moreover, the in-plane hysteresis loop shows a continuous rotation of the magnetization up to saturation, a comportment that is typical for a hard axis of magnetization. In order to extract the relevant anisotropy parameters, we fit the hard-axis loop within the Stoner-Wohlfarth (SW) coherent rotation model [38]. We consider the energy functional $E = (K_{u1} - 2\pi M_s^2)\sin^2\theta_M + K_{u2}\sin^4\theta_M - M_s H\cos\theta_M$, where K_{u1} and K_{u2} are the first- and second-order magnetic anisotropy constants, θ_M is the magnetization polar angle measured from the perpendicular direction and the last term is the Zeeman energy. The experimental data are fitted by minimizing the total energy and using K_1 and K_2 as adjustable parameters. The results of the fit shown in Fig. 5(b) allowed us to determine $K_{u1} = (6.95 \pm 0.2) \times 10^6$ erg/cm^3 and $K_{u2} = (1.6 \pm 0.2) \times 10^6$ erg/cm^3. Most likely that the relatively large K_{u2} has a magnetoelastic origin related to the epitaxial strains in the structure [39]. Using the as-determined constant, we calculate the effective perpendicular anisotropy field $H_k^{\text{eff}} = 2K_{u1}/M_s + 4K_{u2}/M_s - 4\pi M_s$ to be around 0.75 T.

The samples are patterned into the same shape as for the torque measurements (asymmetric Hall crosses), only this time, in order to maximize the current density, the electric current pulses are applied along the narrower arm of the cross. A static in-plane magnetic field (H_x) is applied parallel to the electric current to allow bipolar SOT switching. The magnetization reversal is probed by wide field Kerr microscopy. A perpendicular magnetic field, larger than the coercive field of the device, is applied before injecting the electric pulses to ensure a fully saturated initial state. The image of the saturated state is used as a reference,

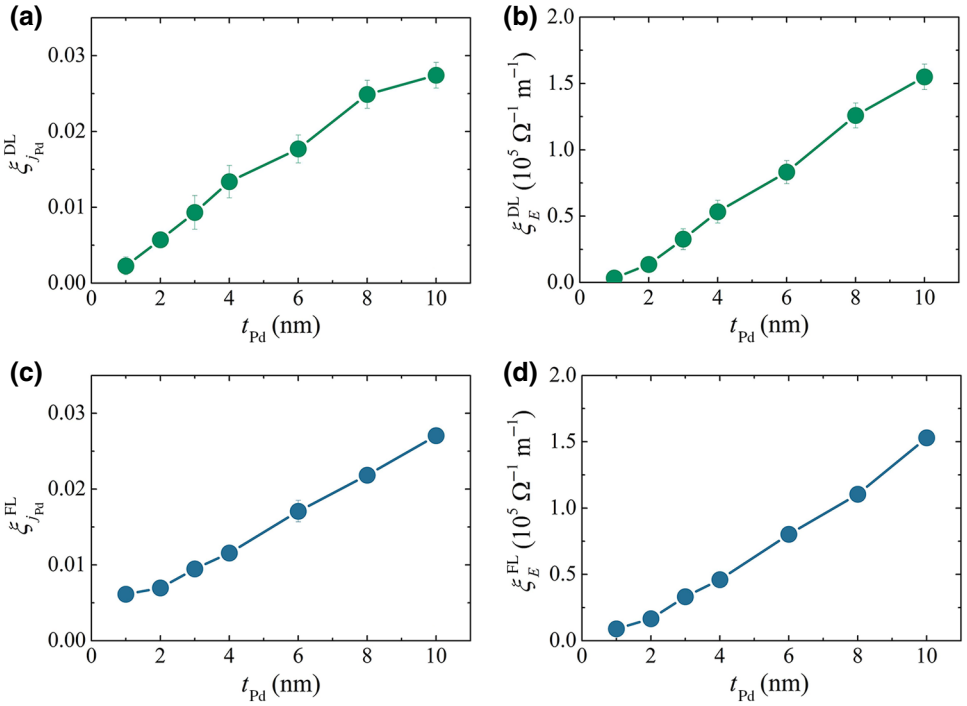

FIG. 4. (a) and (c) the damping-like ($\xi^{DL}_{j_{Pd}}$) and the field-like ($\xi^{FL}_{j_{Pd}}$) SOT efficiencies per unit charge current density through the Pd layer and (b) and (d) the damping-like (ξ^{DL}_{E}) and the field-like (ξ^{FL}_{E}) SOT efficiencies per unit electric field plotted versus the thickness of the Pd layer.

which is subtracted from images obtained after further applying current. The resulting differential images contain only the magnetic contrast of the reversed areas. Figure 6(a) shows the differential Kerr images of magnetic switching for a series of 1000 current pulses of 2.14×10^{12} A/m^2 having a width of 8 ns and with an in-plane magnetic field of 80 mT. The dark (or bright) contrast indicates the regions where the magnetization has reversed. We observe that the switching takes place in the entire area of the narrower arm where the current density is high. The larger areas, where the current density is lower do not switch; their reversal requires larger current pulses. Furthermore, in Fig. 6(b) we plot the reversed area, versus the in-plane applied bias field. We saturate the magnetization each time before changing the value of the in-plane field. As we increase the in-plane field, the reversed area expands.

The Kerr images indicate that the switching occurred progressively by nucleation and domain-wall (DW) propagation (Fig. 6c) from the side of the pad. The first nucleations occur at the edge of the samples possibly due to the Oersted field. The resulting DWs have a Bloch structure, stabilized by the in-plane field (the Pd/CFA interface produces a weak Dzyaloshinskii-Moriya interaction). The SOT produces transverse displacements, as the DWs are magnetized parallel to the current. Note that magnetization reversal by the nucleation and propagation mechanism has already been observed for SOT switching [40,41].

Last but not least, we note that the switching current density in the Pd/CFA heterostructures (2×10^{12} Am^{-2}) is of the same order of magnitude as the current density required for switching the more conventional Pt/Co/AlO$_x$ [4,19] (0.4–1.3×10^{12} Am^{-2}) or

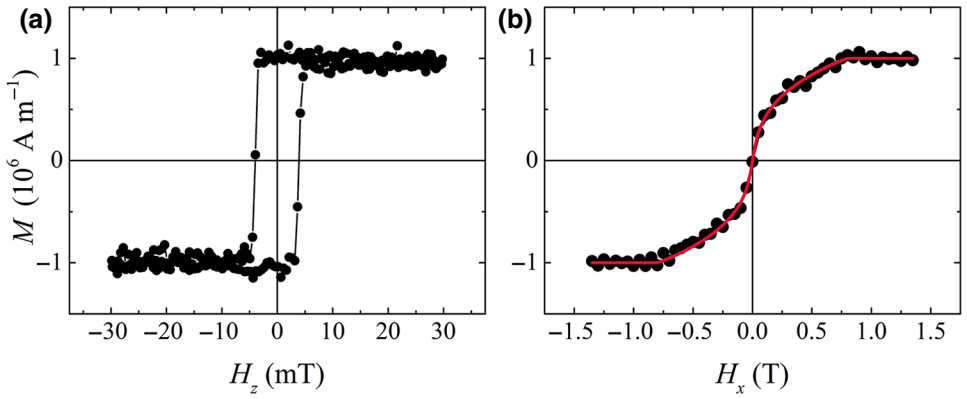

FIG. 5. (a) Perpendicular-to-plane and (b) in-plane hysteresis loops measured for the Pd (8 nm)/ CFA 0.9 nm/ MgO (1 nm) sample, indicating the presence of perpendicular magnetic anisotropy. Points stand for experimental data while the red solid line denotes the result of the fit within the SW model described in the text.

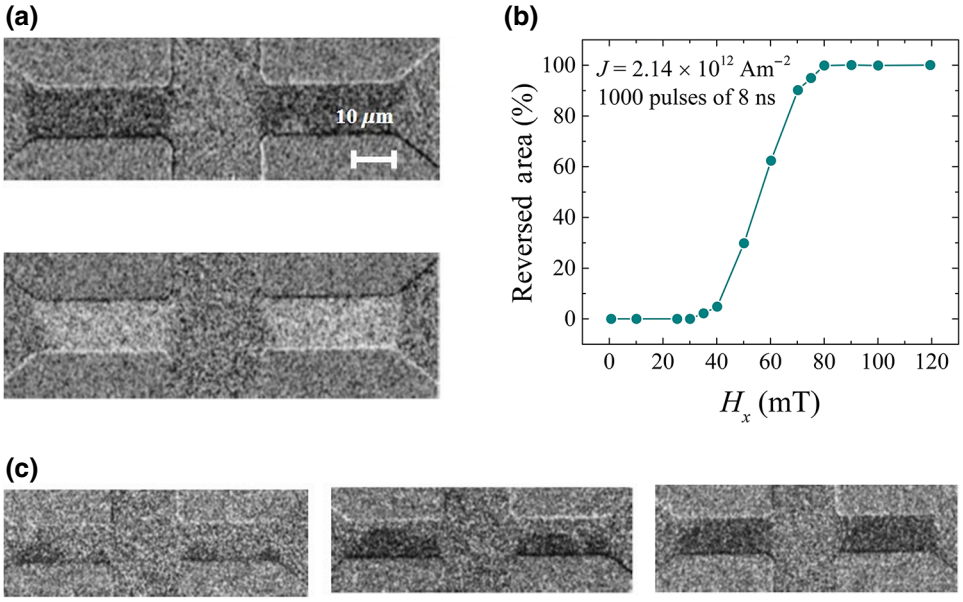

FIG. 6. (a) Differential Kerr microscopy images of the Hall cross showing bipolar magnetic switching by current pulses, from down-to-up magnetization for positive current (dark contrast, top panel) and up-to-down magnetization (bright contrast, bottom panel) for negative current. (b) The reversed area, imaged in (a) top panel, versus the in-plane applied bias field H_x at a constant current density $J \approx 2 \times 10^{12}$ Am^{-2}. The electric current J flows from the right to the left. The direction of H_x is always from the left to the right. (c) Differential Kerr microscopy images of gradual switching. The nucleation occurs first on the edges of the device and the reversal is completed by domain-wall propagation.

high-resistivity Ta/(Co, Fe)B [3] (0.5×10^{12} Am^{-2}) or W/(Co, Fe)B (1.3×10^{12} A/m^2) [25] structures.

III. CONCLUSIONS

We investigate the spin-orbit torques in epitaxial Pd/CFA/MgO magnetic heterostructures grown by magnetron sputtering on (001) single crystal MgO substrates. The dampinglike ξ_E^{DL} ($\xi_{j\mathrm{Pd}}^{\mathrm{DL}}$) and fieldlike ξ_E^{FL} ($\xi_{j\mathrm{Pd}}^{\mathrm{FL}}$) spin-orbit-torque efficiencies per unit electric field (charge current density) show a monotonous increase with increasing the thickness of the Pd layer with no obvious saturation up to 10 nm. The relatively large SOT efficiency is confirmed by SOT switching of perpendicularly magnetized Pd/CFA/MgO heterostructures for current densities of the same order of magnitude as those reported for Pt/Co/AlO_x trilayers. Our results prove that the use of Heusler alloys can combine the energy efficiency of the SOT switching in low-resistivity materials with the possibility of high TMR in perpendicular magnetized MgO-based tunnel junctions, thus offering a platform for the development of energy-efficient SOT memories.

ACKNOWLEDGMENTS

M.S.G, T.P., and M.N. acknowledge the financial support for this work from MRI-CNCS/UEFISCDI through PN-III-P1-1.1-TE-2016-2131-SOTMEM Grant No. 24/02.05.2018. M.A.N, J.N., and I.M.M. acknowledge funding for this work from the European Research Council (ERC) under the European Union's Horizon 2020 research and innovation program (Grant Agreement No. 638653 – Smart Design).

[1] Ioan Mihai Miron, Kevin Garello, Gilles Gaudin, Pierre-Jean Zermatten, Marius V. Costache, Stéphane Auffret, Sébastien Bandiera, Bernard Rodmacq, Alain Schuhl, and Pietro Gambardella, Perpendicular switching of a single ferromagnetic layer induced by in-plane current injection, Nature **476**, 189 (2011).

[2] Luqiao Liu, Chi-Feng Pai, Y. Li, H. W. Tseng, D. C. Ralph, and R. A. Buhrman, Spin-Torque switching with the giant spin hall effect of tantalum, Science **336**, 555 (2012).

[3] Murat Cubukcu, Olivier Boulle, Marc Drouard, Kevin Garello, Can Onur Avci, Ioan Mihai Miron, Juergen Langer, Berthold Ocker, Pietro Gambardella, and Gilles Gaudin, Spin-orbit torque magnetization switching of a three-terminal perpendicular magnetic tunnel junction, Appl. Phys. Lett. **104**, 042406 (2014).

[4] Kevin Garello, Can Onur Avci, Ioan Mihai Miron, Manuel Baumgartner, Abhijit Ghosh, Stéphane Auffret, Olivier Boulle, Gilles Gaudin, and Pietro Gambardella, Ultrafast magnetization switching by spin-orbit torques, Appl. Phys. Lett. **105**, 212402 (2014).

[5] C. Zhang, S. Fukami, H. Sato, F. Matsukura, and H. Ohno, Spin-orbit torque induced magnetization switching in nano-scale Ta/CoFeB/MgO, Appl. Phys. Lett. **107**, 012401 (2015).

[6] Junyeon Kim, Jaivardhan Sinha, Masamitsu Hayashi, Michihiko Yamanouchi, Shunsuke Fukami, Tetsuhiro Suzuki, Seiji Mitani, and Hideo Ohno, Layer thickness dependence of the current-induced effective field vector in TaCoFeBMgO, Nat. Mater. **12**, 240 (2012).

[7] Chaoliang Zhang, Michihiko Yamanouchi, Hideo Sato, Shunsuke Fukami, Shoji Ikeda, Fumihiro Matsukura, and Hideo Ohno, Magnetotransport measurements of current induced effective fields in Ta/CoFeB/MgO, Appl. Phys. Lett. **103**, 262407 (2013).

[8] Kevin Garello, Ioan Mihai Miron, Can Onur Avci, Frank Freimuth, Yuriy Mokrousov, Stefan Blügel, Stéphane Auffret, Olivier Boulle, Gilles Gaudin, and Pietro Gambardella, Symmetry and magnitude of spin–orbit torques in ferromagnetic heterostructures, Nat. Nanotechnol. **8**, 587 (2013).

[9] Can Onur Avci, Kevin Garello, Corneliu Nistor, Sylvie Godey, Belén Ballesteros, Aitor Mugarza, Alessandro Barla, Manuel Valvidares, Eric Pellegrin, Abhijit Ghosh, Ioan Mihai Miron, Olivier Boulle, Stephane Auffret, Gilles Gaudin, and Pietro Gambardella, Fieldlike and antidamping spin-orbit torques in as-grown and annealed Ta/CoFeB/MgO layers, Phys. Rev. B **89**, 214419 (2014).

[10] Can Onur Avci, Kevin Garello, Johannes Mendil, Abhijit Ghosh, Nicolas Blasakis, Mihai Gabureac, Morgan Trassin, Manfred Fiebig, and Pietro Gambardella, Magnetoresistance of heavy and light metal/ferromagnet bilayers, Appl. Phys. Lett. **107**, 192405 (2015).

[11] Chi-Feng Pai, Luqiao Liu, Y. Li, H. W. Tseng, D. C. Ralph, and R. A. Buhrman, Spin transfer torque devices utilizing the giant spin Hall effect of tungsten, Appl. Phys. Lett. **101**, 122404 (2012).

[12] Chi-Feng Pai, Minh-Hai Nguyen, Carina Belvin, Luis Henrique Vilela-Leão, D. C. Ralph, and R. A. Buhrman, Enhancement of perpendicular magnetic anisotropy and transmission of spin-Hall-effect-induced spin currents by a Hf spacer layer in W/Hf/CoFeB/MgO layer structures, Appl. Phys. Lett. **104**, 082407 (2014).

[13] Soonha Cho, Seung-heon Chris Baek, Kyeong-Dong Lee, Younghun Jo, and Byong-Guk Park, Large spin Hall magnetoresistance and its correlation to the spin-orbit torque in W/CoFeB/MgO structures, Sci. Rep. **5**, 14668 (2015).

[14] M. S. Gabor, T. Petrisor, R. B. Mos, A. Mesaros, M. Nasui, M. Belmeguenai, F. Zighem, and C. Tiusan, Spin–orbit torques and magnetization switching in W/Co 2 FeAl/MgO structures, J. Phys. D: Appl. Phys. **49**, 365003 (2016).

[15] Kai-Uwe Demasius, Timothy Phung, Weifeng Zhang, Brian P. Hughes, See-Hun Yang, Andrew Kellock, Wei Han, Aakash Pushp, and Stuart S. P. Parkin, Enhanced spin–orbit torques by oxygen incorporation in tungsten films, Nat. Commun. **7**, 10644 (2016).

[16] C. Zhang, S. Fukami, K. Watanabe, A. Ohkawara, S. DuttaGupta, H. Sato, F. Matsukura, and H. Ohno, Critical role of W deposition condition on spin-orbit torque induced magnetization switching in nanoscale W/CoFeB/MgO, Appl. Phys. Lett. **109**, 192405 (2016).

[17] Luqiao Liu, Takahiro Moriyama, D. C. Ralph, and R. A. Buhrman, Spin-Torque Ferromagnetic Resonance Induced by the Spin Hall Effect, Phys. Rev. Lett. **106**, 036601 (2011).

[18] Luqiao Liu, O. J. Lee, T. J. Gudmundsen, D. C. Ralph, and R. A. Buhrman, Current-Induced Switching of Perpendicularly Magnetized Magnetic Layers Using Spin Torque from the Spin Hall Effect, Phys. Rev. Lett. **109**, 096602 (2012).

[19] Can Onur Avci, Kevin Garello, Ioan Mihai Miron, Gilles Gaudin, Stéphane Auffret, Olivier Boulle, and Pietro Gambardella, Magnetization switching of an MgO/Co/Pt layer by in-plane current injection, Appl. Phys. Lett. **100**, 212404 (2012).

[20] Hwang-Rae Lee, Kyujoon Lee, Jaehun Cho, Young-Ha Choi, Chun-Yeol You, Myung-Hwa Jung, Frédéric Bonell, Yoichi Shiota, Shinji Miwa, and Yoshishige Suzuki, Spin-orbit torque in a bulk perpendicular magnetic anisotropy Pd/FePd/MgO system, Sci. Rep. **4**, 6548 (2014).

[21] Abhijit Ghosh, Kevin Garello, Can Onur Avci, Mihai Gabureac, and Pietro Gambardella, Interface-Enhanced Spin-Orbit Torques and Current-Induced Magnetization Switching of Pd/Co/AlO_x Layers, Phys. Rev. Appl. **7**, 014004 (2017).

[22] Minh-Hai Nguyen, Chi-Feng Pai, Kayla X. Nguyen, David A. Muller, D. C. Ralph, and R. A. Buhrman, Enhancement of the anti-damping spin torque efficacy of platinum by interface modification, Appl. Phys. Lett. **106**, 222402 (2015).

[23] S. V. Aradhya, G. E. Rowlands, J. Oh, D. C. Ralph, and R. A. Buhrman, Nanosecond-Timescale Low energy switching of In-plane magnetic tunnel junctions through dynamic Oersted-field-assisted spin Hall effect, Nano Lett. **16**, 5987 (2016).

[24] M. Cubukcu, O. Boulle, N. Mikuszeit, C. Hamelin, T. Brächer, N. Lamard, M. Cyrille, L. Buda-Prejbeanu, K. Garello, I. M. Miron, O. Klein, G. de Loubens, V. V. Naletov, J. Langer, B. Ocker, P. Gambardella, and G. Gaudin, Ultra-Fast perpendicular spin–orbit torque MRAM, IEEE Trans. Magn. **54**, 1 (2018).

[25] K. Garello, F. Yasin, S. Couet, L. Souriau, J. Swerts, S. Rao, S. Van Beek, W. Kim, E. Liu, S. Kundu, D. Tsvetanova, K. Croes, N. Jossart, E. Grimaldi, M. Baumgartner, D. Crotti, A. Fumémont, P. Gambardella, and G. S. Kar, in Presented at the 2018 IEEE Symposium on VLSI Circuits (2018). (unpublished).

[26] S. Ikeda, K. Miura, H. Yamamoto, K. Mizunuma, H. D. Gan, M. Endo, S. Kanai, J. Hayakawa, F. Matsukura, and H. Ohno, A perpendicular-anisotropy CoFeB–MgO magnetic tunnel junction, Nat. Mater. **9**, 721 (2010).

[27] William H. Butler, Tunneling magnetoresistance from a symmetry filtering effect, Sci Technol. Adv. Mater. **9**, 014106 (2008).

[28] B. Dieny and M. Chshiev, Perpendicular magnetic anisotropy at transition metal/oxide interfaces and applications, Rev. Mod. Phys. **89**, 025008 (2017).

[29] M. S. Gabor, T. Petrisor, C. Tiusan, and M. Hehn, Magnetic and structural anisotropies of Co_2FeAl Heusler alloy epitaxial thin films, Phys. Rev. B **84**, 134413 (2011).

[30] Zhenchao Wen, Hiroaki Sukegawa, Shinya Kasai, Masamitsu Hayashi, Seiji Mitani, and Koichiro Inomata, Magnetic tunnel junctions with perpendicular anisotropy using a Co_2FeAl full-heusler alloy, Appl. Phys. Express **5**, 063003 (2012).

[31] Zhenchao Wen, Hiroaki Sukegawa, Takao Furubayashi, Jungwoo Koo, Koichiro Inomata, Seiji Mitani, Jason Paul Hadorn, Tadakatsu Ohkubo, and Kazuhiro Hono, A 4-fold-symmetry hexagonal ruthenium for magnetic heterostructures exhibiting enhanced perpendicular magnetic anisotropy and tunnel magnetoresistance, Adv. Mater. **26**, 6483 (2014).

[32] M. S. Gabor, M. Belmeguenai, T. Petrisor, C. Ulhaq-Bouillet, S. Colis, and C. Tiusan, Correlations between structural, electronic transport, and magnetic properties of $Co_2FeAl_{0.5}Si_{0.5}$ Heusler alloy epitaxial thin films, Phys. Rev. B **92**, 054433 (2015).

[33] Ung Hwan Pi, Kee Won Kim, Ji Young Bae, Sung Chul Lee, Young Jin Cho, Kwang Seok Kim, and Sunae Seo, Tilting of the spin orientation induced by Rashba effect in ferromagnetic metal layer, Appl. Phys. Lett. **97**, 162507 (2010).

[34] Masamitsu Hayashi, Junyeon Kim, Michihiko Yamanouchi, and Hideo Ohno, Quantitative characterization of the spin-orbit torque using harmonic Hall voltage measurements, Phys. Rev. B **89**, 144425 (2014).

[35] I. M. Miron, P. J. Zermatten, G. Gaudin, S. Auffret, B. Rodmacq, and A. Schuhl, Domain Wall Spin Torquemeter, Phys. Rev. Lett. **102**, 137202 (2009).

[36] Can Onur Avci, Kevin Garello, Mihai Gabureac, Abhijit Ghosh, Andreas Fuhrer, Santos F. Alvarado, and Pietro Gambardella, Interplay of spin-orbit torque and thermoelectric effects in ferromagnet/normal-metal bilayers, Phys. Rev. B **90**, 224427 (2014).

[37] Minh-Hai Nguyen, D. C. Ralph, and R. A. Buhrman, Spin Torque Study of the Spin Hall Conductivity and Spin Diffusion Length in Platinum Thin Films with Varying Resistivity, Phys. Rev. Lett. **116**, 126601 (2016).

[38] Edmund Clifton Stoner and E. P. Wohlfarth, A mechanism of magnetic hysteresis in heterogeneous alloys, Philosophical Transactions of the Royal Society of London, Series A, Math. Phys. Sci. **240**, 599 (1948).

[39] Kin Ha and Robert C. O'Handley, Magnetization canting in epitaxial Cu/Ni/Cu/Si(001) films, J. Appl. Phys. **87**, 5944 (2000).

[40] J.-C. Rojas-Sánchez, P. Laczkowski, J. Sampaio, S. Collin, K. Bouzehouane, N. Reyren, H. Jaffrès, A. Mougin, and J.-M. George, Perpendicular magnetization reversal in Pt/[Co/Ni]3/Al multilayers via the spin hall effect of Pt, Appl. Phys. Lett. **108**, 082406 (2016).

[41] Manuel Baumgartner, Kevin Garello, Johannes Mendil, Can Onur Avci, Eva Grimaldi, Christoph Murer, Junxiao Feng, Mihai Gabureac, Christian Stamm, Yves Acremann, Simone Finizio, Sebastian Wintz, Jörg Raabe, and Pietro Gambardella, Spatially and time-resolved magnetization dynamics driven by spin–orbit torques, Nat. Nanotechnol. **12**, 980 (2017).